Wear xxx (xxxx) xxx

Contents lists available at ScienceDirect

Wear

journal homepage: www.elsevier.com/locate/wear

Abrasive wear resistance of Ti-6AL-4V obtained by the conventional manufacturing process and by electron beam melting (EBM)

P. Herrera [a], E. Hernandez-Nava [b], R. Thornton [c,d], T. Slatter [a,*]

[a] Department of Mechanical Engineering, The University of Sheffield, Mappin Street, Sheffield, UK
[b] Department of Materials Science & Engineering, The University of Sheffield, Mappin Street, Sheffield, UK
[c] School of Engineering, University of Leicester, University Road, Leicester, UK
[d] Warwick Manufacturing Group (WMG), The University of Warwick, Coventry, UK

ARTICLE INFO

Keywords:
Abrasive wear
ASTM G65
Titanium alloy Ti–6Al–4V
Electron beam melting (EBM)

ABSTRACT

Ti–6Al–4V is one of the most used commercial titanium alloys, in part due to properties that are desirable in high value sectors such as the aerospace industry, such as good strength-to-weight ratio and corrosion resistance. These are of importance in gas turbine engines and structural components, where titanium alloys complement heavier steel or nickel alloys. It is also a good candidate to be used in the manufacturing of prostheses, since it has good biocompatibility, but applications in other areas are limited due to its poor bulk wear resistance.

Conventionally processed Ti-6AL-4V is typically used, however additive manufacturing (AM) techniques such as electron beam melting (EBM) can also be applied to this alloy. These techniques are increasingly attractive across many industries because of geometrical freedom and control of mechanical properties, both key, for example, to the successful production of highly personalised prostheses and complex thermofluids channels in aerospace and automotive components. Parts produced by EBM are typically denser than those obtained by other AM processes, but still experience increased wear over their traditionally obtained equivalents, particularly in sliding, thus surface treatment is common.

This work compares the wear observed when specimens manufactured by either conventionally or EBM were subjected to abrasion via means of a dry sand-rubber wheel tribometer capable of testing to the ASTM G65 test method. The specimens and resulting wear scars were characterised (hardness, grain size, roughness) and details of the wear mechanism(s) identified. The EBM specimens exhibited much greater wear, over twice that of the conventionally obtained specimens, and feature significantly more scratches.

Although there are several studies variously considering two-body sliding wear and the efficacy of surface treatments of this type of alloy, this work addresses the paucity of information about the comparative abrasive wear performance of the alloy obtained via the two process routes.

1. Introduction

Ti–6Al–4V (colloquially known as “Ti64”) is an alpha-beta titanium alloy containing aluminium (≈6% wt.) and vanadium (≈4% wt.) as the main alloying elements. It is the most commonly used commercial titanium alloy grade [1–3]. Its broad applicability comes from its excellent corrosion resistance, good machinability, and good strength-to-weight ratio. These advantages allow the implementation of this alloy in many types of different applications, particularly in the automotive, aerospace, and biomechanical medical device industries. It has a density of up to 50% of steel or nickel alloys, therefore having wide application in areas in which the low weight of parts is extremely important. Another important characteristic of this material is its biocompatibility [2,4], making it a good candidate to be used in direct contact with bones or tissues. Due to this alloy’s poor wear resistance, particularly in sliding (including abrasion) it is usually submitted to surface treatments when a better wear resistance is needed during the application [1,5–7].

Conventional Ti64 (i.e. material that is cast, hot rolled or wrought and then variously annealed) is widely used in the aerospace industry, and also used in areas in which low weight is considered important, like motorsport or unmanned aerial vehicles [3]. In recent years additive manufacturing (AM), which consists (in a simplified manner) of building shapes one layer at time, has gathered more focus and attention, since it

* Corresponding author.
E-mail address: tom.slatter@sheffield.ac.uk (T. Slatter).

https://doi.org/10.1016/j.wear.2023.204879
Received 21 September 2022; Received in revised form 19 January 2023; Accepted 7 February 2023
Available online 6 April 2023

makes possible to efficiently create complex shapes. One type of AM is electron beam melting (EBM), in which the alloy powder is layered in a vacuum environment, and each layer is melted according to the design, using a powerful electron beam, producing a dense solid part. Any unmelted alloy powder is later removed and can be re-utilised.

This makes possible the manufacturing of near-solid parts with complex shapes and good tolerances, which are characteristics required in high-performance engineering components and medical implants. Compared to the conventionally obtained Ti64, however, Ti64 produced by EBM typically presents a higher cost per part manufactured. It is therefore currently limited in its usages to these specific applications where cost is not one of the main factors when selecting the material as either the benefits outweigh the cost, or enable the design to be manufactured at all due to their complex geometry.

Due to the thermomechanical differences in process routes, AM parts exhibit significantly different microstructures to those manufactured by conventional means and, hence, often have different mechanical and tribological properties. Conventional Ti64 that has been heavily worked (such as the hot rolled and annealed material used in this study) commonly displays globular α phase and transformed β. By contrast, Ti64 produced by EBM has a columnar prior β morphology, which transforms to a microstructure of diffusional α + β. This transformation results in fine Widmanstätten α laths with no preferred texture, which is generally thought to be beneficial in terms of reducing anisotropy in material properties. EBM materials have been shown to follow a Hall-Petch type relationship with strength increasing with decreasing α lath size and α colony scale factor [8]. Strength of EBM Ti64 is therefore significantly dependent on the process parameters adopted, and it might be expected that hardness and abrasive wear resistance (assuming linear wear behaviour) may also be closely correlated.

The process routes used in this study were selected due to the lack of literature that compares the wear resistance of Ti64 and the EBM Ti64 directly. The possibility of submitting this important alloy, produced using different techniques, to the same mechanical tests that are a proxy for some of the contacts experienced in the field, therefore made it an important research subject.

2. Materials and methods

With the aim to characterise the abrasive wear resistance of Ti64 alloy in its conventionally and EBM obtained condition, standard samples were manufactured, mechanically characterised, and subjected to an abrasive wear test. In the case of this study, the chosen test was the abrasive wear test ASTM G65 [9], which uses a rubber wheel and sand, as the abrasive medium, and is defined as a three body abrasive test and replicates the wear mechanism commonly experienced by this alloy when used in engineering components and systems (Section 1).

2.1. Titanium test samples

Two types of titanium alloy were used: a Ti64 that was cast before being hot rolled into plate and then annealed (referred to as 'conventionally obtained', 'conventional' or 'Ti64' here); a Ti64 powder used in an electron beam melting additive manufacturing process (EBM - specifically the Arcam AB variant) (referred to as 'EBM Ti64' or 'ETi64' here). The composition, supplied by the manufacturer, of the Ti64 and the EBM Ti64 used in the tested samples are presented on Table 1.

Rectangular test samples were manufactured via both process routes to be as close as possible to the standard ASTM G65 geometry (Fig. 1a), with the surface to be tested machined to be flat within 0.125 mm, and with a ground surface roughness of no greater than 0.8 μm, in this case confirmed by means of a column-type surface roughness contact profilometer (a Mitutoyo SJ500), which used a 2 μm 60° diamond tip stylus. The conventional Ti64 was obtained from a plate of the material, which had the same thickness as the sample, and was machined to present the required dimensions and surface finish. AM samples were prepared from a Ti64 plasma atomised powder, particle size distribution (PSD) of 45–106 μm.

Table 1
Chemical composition[a] (wt.%) for the Ti64 and the EBM Ti64.

	Vanadium	Aluminium	Iron	Oxygen	Titanium
Ti64	3.95	6.24	0.18	0.16	Balance
EBM Ti64	3.94	6.45	0.19	0.12	Balance

[a] Chemical composition information supplied by the manufacturer.

The manufacturing of AM specimens was carried out in an Arcam A2 machine (software version V.3.2.121) using speed function 36 in "Autocalc" mode, subsequently referred to as the "standard parameters". The true values of the beam parameters cannot be disclosed as they are commercially sensitive and protected by the technology manufacturer. The process commenced at the point at which the equipment reached 1×10^{-4} mbar in vacuum and this was further controlled at 1×10^{-3} mbar throughout the process (using helium). The preheat-melting sequence started once the substrate plate was initially heated up to 730 °C. Fig. 1b shows the schematic of the resulting AM sample in its built orientation, which used one of the sides (76 × 8 mm) as a base.

The samples required for chemical composition analysis, metallography and hardness tests were sectioned and finished according to the needed conditions for each of the tests, from the main batch of test samples also used for the wear tests. All tests were performed on the same face of each of the materials, i.e. each of the samples used on the characterisation has the same orientation of the samples used in the wear test experiment. To simplify the comparison of the results, the conventionally obtained samples will be referred as "Ti64" and the EBM obtained samples will be referred as "ETi64" in the following tables and figures.

2.2. Hardness and micro-hardness

Vickers macro-hardness (HV) testing was chosen due to its capacity of utilising the same indenter for different scales of hardness, only needing to change the applied load accordingly. The measurements were performed on all the samples that were later used in the wear tests.

To ensure that the hardness measurement could be compared, all of the TI64 and ETi64 samples hardness tests were performed in the same session (same day). The tests were performed on the same face (25 × 76 mm) as the wear test and the samples were selected at random. Each of the samples was tested four times, which resulted in 24 measurements for each of the sample groups (conventional and EBM). A load of 20 kgf was chosen to create large indentations relative to the measurement resolution and therefore minimise errors in the calculated hardness number.

An automated hardness tester (EMCOTest Durascan) was used to measure the Vickers microhardness. A load of 0.1 kgf was chosen (as preliminary tests determined that this was the smallest test force that would still present a measurable and reliable indentation) and the measurement was taken using a 9-point matrix (3 × 3) produced indentations as expected. Smaller samples were sectioned, mounted and polished, since a flat clean surface is needed for this procedure.

2.3. Materials characterisation

The preparation of the samples for the metallographic analysis was conducted according to the recommended procedure for titanium alloys from the consumables' supplier (MetPrep, U.K.). Smaller samples (10 mm cubes) were sectioned from the original samples using a precision cutting machine with an abrasive disc, being thoroughly cooled to decrease the heat generated and its effects on the sample.

The smaller samples were hot mounted in a conductive Bakelite resin with carbon filler, to allow for electro-etching and scanning electron microscopy (SEM) visualization techniques. Each sample was ground

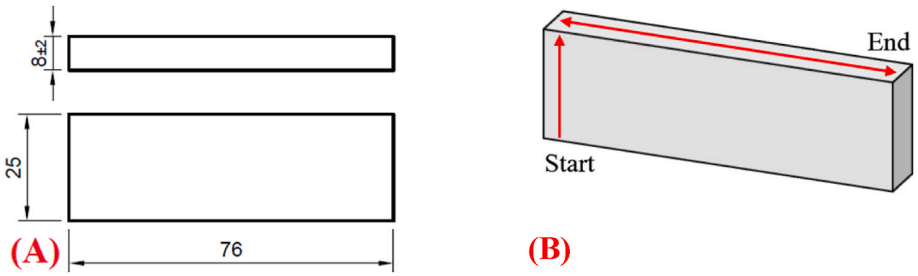

Fig. 1. Samples for the abrasive wear rig: (A) Standard G65 rectangular sample, (B) Schematic of the directions of the EBM Ti64 additive process.

and polished on an automated machine (Buehler Automet) e, to ensure good repeatability in sample preparation.

Both Ti64 and ETi64 samples were prepared in the same way. Samples were ground for 3 min using a selection of water lubricated abrasive papers (grit 600, 1200 and 2000) and, after, were polished for 10 min using a 9 μm diamond suspension on a cloth and a final polishing using colloidal silica for 6 min. Samples were cleaned and dried between each of the grinding and polishing steps to minimise particulate contamination.

Two SEM instruments were used to perform the scanning electron microscopy according to the specific needs of the analysis; a benchtop model (Hitachi TM3030), and a conventional SEM (FEI Quanta 650), which were used to generate lower and higher resolution images, respectively.

2.4. Abrasive wear testing

An in-house (University of Sheffield, U.K.) designed dry sand-rubber wheel (DSRW) type abrasive wear test apparatus (Fig. 2) was used throughout this work. It is capable of testing to ASTM G65-16 (Standard Test Method for Measuring Abrasion Using the Dry Sand/Rubber Wheel Apparatus) [9] and was designed to the recommendations contained therein. The wheels used are of the newer neoprene rubber type, as defined in ASTM G65, and are the same physical dimensions as the one presented in the standard.

The lever mechanism was designed such to facilitate the smooth unloading of the sample by ensuring that the force necessary to unload it using the lever is significantly less than the weight of the load applied to the end of the load arm. The form factor of this design is more compact than presented in the standard but this does not impact the parameters of the test (load, wheel rotational speed, sand flow rate were confirmed to be compliant by a loadcell, a tachometer, and time taken for a known mass of sand to be collected, respectively).

It should be noted here that due to the different wear responses observed during initial testing of the Ti64 and ETi64 samples (Sections 3.3-3.4), two of the test method variants defined within ASTM G65 were used. It was expected that ASTM G65 Method A, which defines that 6000 revolutions is to be used, would be used throughout but it became apparent that Method B, which defines 2000 revolutions should be used, was more suitable to produce a test valid within the context of the standard for ETi64 samples. As defined in ASTM G65, for all tests a load of 130 N was applied between the sample and rubber wheel, and the rotational speed maintained at 200 ± 10 rpm.

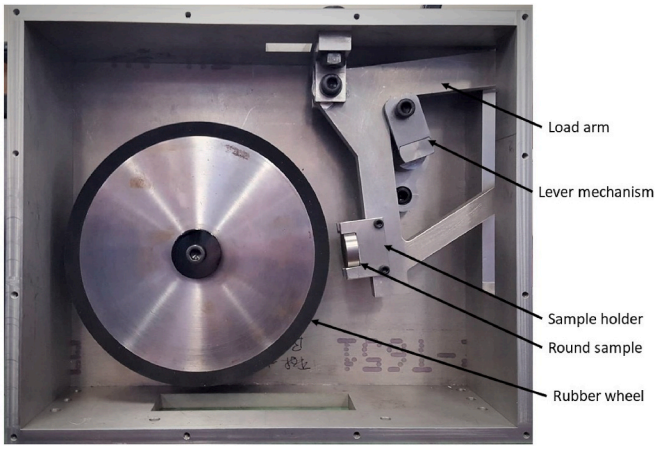

Fig. 2. Initial assembly of the DSRW Rig.

2.5. Roughness and non-contact profilometry

To measure the test specimen surface and to make a volumetric determination of the mass loss from the worn surfaces, a 3D non-contact profilometer (focus-variation type, Alicona InfiniteFocus SL, MeasureSuite) was used. The 5x and 10x objectives were used according to the size of the wear scar and to achieve a good resolution within the dataset.

3. Results

3.1. Hardness and micro-hardness

The hardness results are as expected for the Ti64 alloys, and the measurements performed had excellent repeatability. Due to the number of measurements performed (24 in each case), and the relatively small standard deviation presented, the standard error was always lower than 0.5% of the total hardness value. The results are presented in Table 2 and Fig. 3.

As mentioned, these samples were also submitted to an automated Vickers micro-hardness measurement. It was desirable to identify any differences in indentation resistance due to microstructural features as Ti–6Al–4V is an α+β alloy with a transformed grain size, and strengthening predominantly due to the size of alpha plates [10]. The results for the micro-hardness measurements are presented in Table 3 and Fig. 4.

3.2. Microstructural characterisation

To measure the grain size, the images obtained from an optical microscope (using cross-polarised light) were used. The results for each material are presented in Table 4.

The results were similar to others previously reported. For ETi64, a size of approximately 2 μm has been reported for similar EBM systems [11], whereas microstructural features in conventionally obtained Ti64 can vary depending on post processing conditions. Results suggest that the contribution to wear resistance due to grain size would be expected

Table 2
Titanium samples Vickers hardness (HV 20) values.

Sample	Average Hardness [HV20]	Standard Deviation (σ)	Standard Error ($\sigma_{\bar{x}}$)	% Standard Error
Ti64	383.42	6.09	1.24	0.32%
ETi64	373.65	6.28	1.28	0.34%

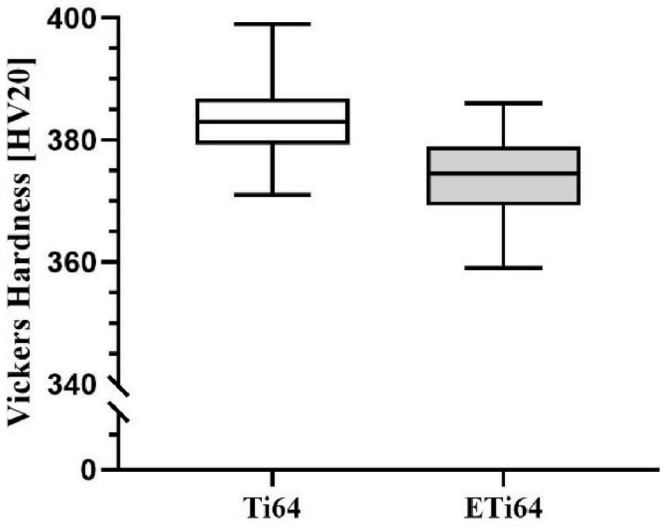

Fig. 3. Titanium samples Vickers hardness (HV 20).

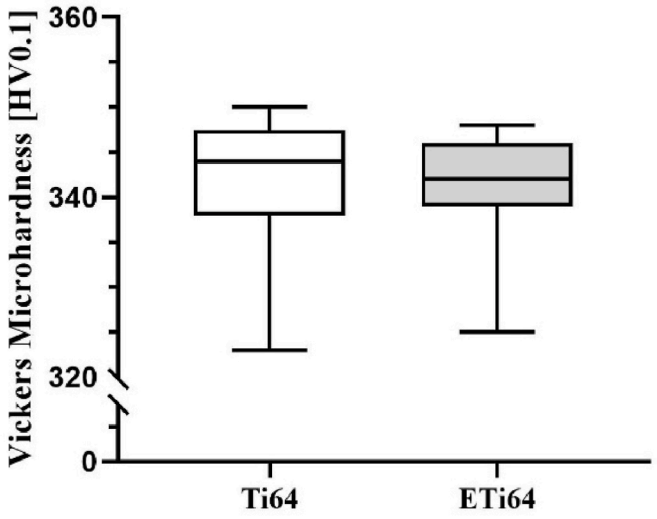

Fig. 4. Titanium samples Vickers micro-hardness (HV0.1).

Table 3
Titanium samples Vickers micro-hardness (HV 0.1) values.

Sample	Average Hardness [HV0.1]	Standard Deviation (σ)	Standard Error (σ $\bar{x}$)	% Standard Error
Ti64	341.36	8.22	2.74	0.80%
ETi64	340.79	6.89	2.30	0.67%

The microhardness results have a small standard deviation and an excellent standard error, since it is smaller than 1% of the measured microhardness for all the obtained values. While ETi64 presented a slightly lower mean macro-hardness (by about 10 HV20), the micro-hardness results from both sets of samples were effectively equal.

to be fairly similar.

While the Ti–6Al–4V is strengthened by a variety of mechanisms (e.g. prior grain size, transformed microstructure, solute content and work hardening [12]) determining the specific contribution that each makes to wear resistance is out of the scope of this manuscript.

In AM components, it is important to characterise if defects due to lack of fusion are present in the material. The porosity of the titanium samples was measured to better understand the wear behaviour of the EBM obtained material. Two polished samples of each material were scanned using an optical microscope and a Clemex system (image acquisition & associated software) to analyse and quantify the pores present. Examples of the images, illustrating the size and distribution of the pores pores (presenting as the dark spots in the images), used in this process are presented in the Appendix and the results are presented in Table 5. They clearly show that EBM Ti64 is significantly more porous (6.8x more pores per area) than the conventionally obtained equivalent.

Fig. 5 shows examples of the general microstructure obtained using cross-polarised lens in an optical microscope for a Ti64 sample, with Fig. 6 showing the equivalent micrographs for a ETi64 sample. Following the metallographic preparation previously described, there was no need to further etch the samples to analyse the microstructure and the effect of the wear in the subsurface, as the α microstructure could be clearly seen after the polishing Since the images are relatively low resolution, as the study focuses on macroscale abrasion, the β phase do not show distinctively. It should also be noted here that the pores

Table 4
Ti64 and ETi64 grain size.

Sample	Average Intercept [μm]	ASTM Grain Size [G]
ETi64	1.635	15.2
Ti64	3.034	13.5

Table 5
Measured and calculated pore count for Ti64 and ETi64.

Sample	Pore average length [μm]	Pore average area [μm^2]	Pores per area [pores/μm^2]	Pore % of total area
Ti64	10.05	56.65	0.239E-06	0.00136%
ETi64	17.74	253.49	1.626E-06	0.04121%

visible in Figs. 5 and 6 are some of the smaller sized pores present in the material as these areas were selected primarily to illustrate the microstructure. The mean sizes of the pores (Table 5) are an order of magnitude larger than the rest of the microstructural features (Table 4) so many of the pores present would obscure the microstructure at this magnification.

The micrographs presented show that the conventional Ti64 is composed of equiaxed α grains (globules) of similar average sizes, as is common for this type of titanium alloy when submitted to hot rolling, such as here. As seen in Fig. 5, some silica particles that got stuck inside of the pores during the final stage of polishing are present and, when submitted to a high intensity light, appear as white dots. The few pores present in these samples are shown as dark rounder spots and as pores can vary in size, an area with smaller pores was chosen to illustrate the microstructure, since an area including any average measured size pores would mostly only show the pores themselves.

By contrast, the EBM obtained Ti64 samples presented predominantly lamellar α grains (fine plates), which are commonly observed in Ti6–4Al–4V manufactured by EBM. As widely described by others, it is composed of columnar prior grains parallel to the build direction with a fine α+β transformed microstructure in the form of lamellar plates.

While the former β structure is affected by the directional heat gradient, so leaving a columnar morphology, the transformed

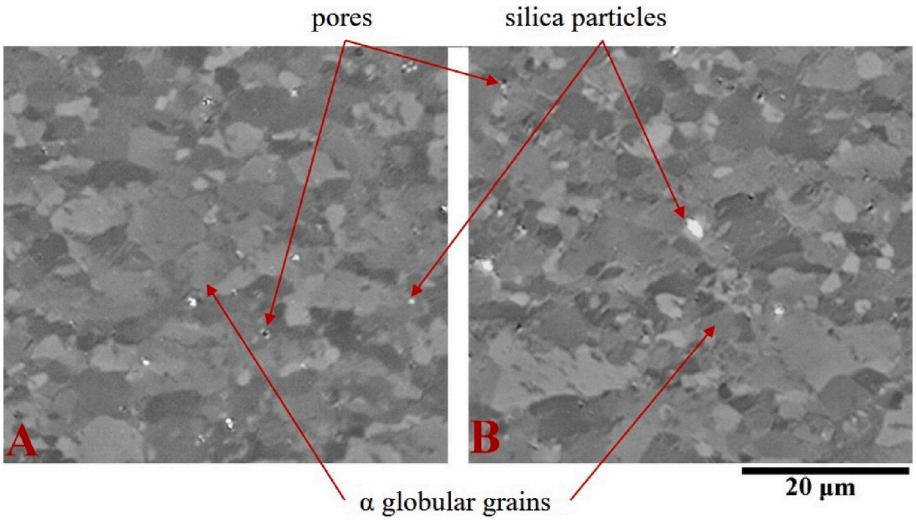

Fig. 5. Two examples (A, B) of the microstructure of conventionally obtained Ti64.

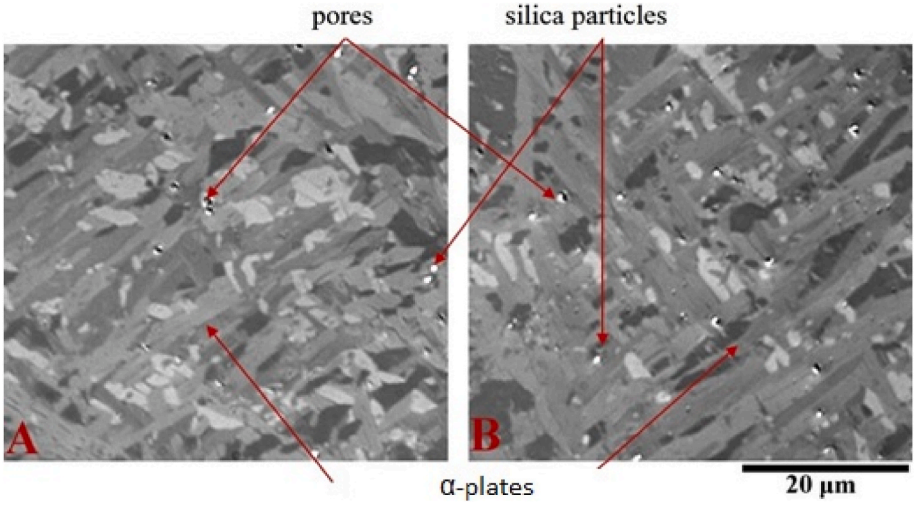

Fig. 6. Two examples (A, B) of the microstructure of EBM obtained Ti64.

Table 6
Outline of the ASTM G65 test methods for the titanium alloys.

Test Method	Revolutions	Load Applied [N]	Wheel speed [rpm]
A[a]	6000	130	200
B	2000	130	200

[a] Initial tests conducted on all samples; extreme wear scar observed for EBM Ti64 samples.

microstructure (the fine plate morphology), is due to the fast cooling in the EBM process. These lamellar structures develop from a larger β grain that forms during solidification and transforms, during cooling, into the α+β lamellar grains observed here, and by others.

3.3. Wear volume

For abrasive wear testing, the Ti64 samples were subjected to ASTM

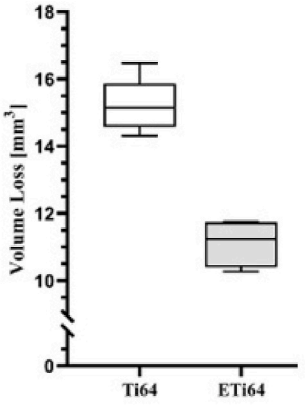

Fig. 7. Titanium samples abrasive wear volume loss [mm^3]: Ti64 Method A; ETi64 Method B.

Table 7
Titanium samples abrasive wear test results.

Sample	Test Method	Number of Tests	Mass Loss [mg]	Volume Loss [mm^3]	Standard Deviation (σ)	Standard Error (σ $\bar{x}$)	% Standard Error
Ti64	A	5	67.360	15.205	0.801	0.401	2.63%
ETi64	B	4	49.285	11.125	0.729	0.364	3.28%

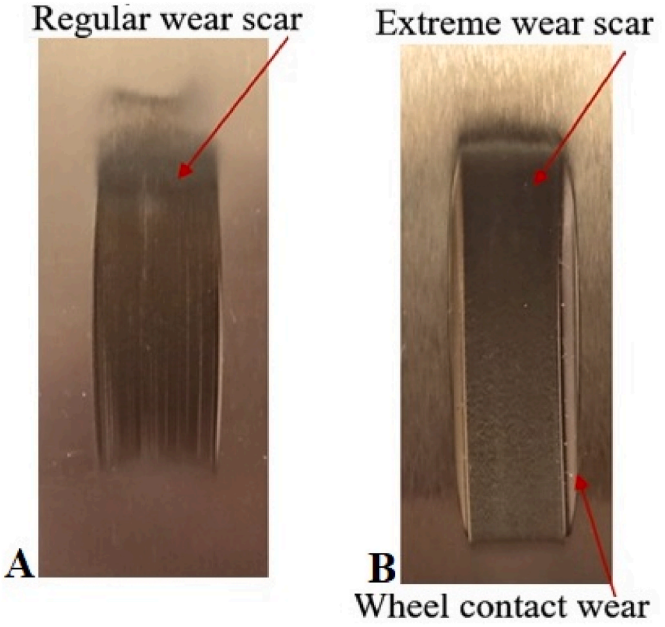

Fig. 8. Typical wear scar for the abrasive wear test method A: (A) Ti64; (B) ETi64.

G65 Test Method A (6000 cycles). When the EBM Ti64 samples were also subjected to Test Method A (6000 cycles), extremely large wear scars were formed, compared to the examples provided in the standard, thus the test deemed invalid for ASTM G65. Once the wear from the wheel-sand-sample contact had become greater than is normally expected of this type of test, there was then contact between the edge of the rubber wheel (i.e. beyond that of the width of the flowing sand curtain) and sample (this is further discussed in Section 4). Hence, data for ETi64 samples presented here comes from Test Method B (2000 cycles), which was found to produce a similar wear volume to the Ti64 samples after 6000 cycles. The outline for the ASTM G65 tests is shown in Table 6. Samples were tested in a random order and the results are presented in Fig. 7 and Table 7.

Both sample groups presented a standard error smaller than 4%, indicating good repeatability. Accounting for the difference in test durations, the mean wear rate of ETi64 samples was determined to be 120% greater than Ti64 samples (0.0055 vs 0.0025 mm^3 rev^{-1}).

3.4. Wear scars

The typical wear scars for the Ti64 and ETi64 samples subjected to test method A (130 N and 6000 cycles) are shown in Fig. 8.

All wear scars created during this study were of the general form and with the in-scar surface features (e.g. long scratches) typically expected from ASTM G65 testing, thus confirming three-body abrasive wear had occurred. While the conventionally cast, rolled, and annealed Ti64 presented a regular wear scar very similar to those shown in the

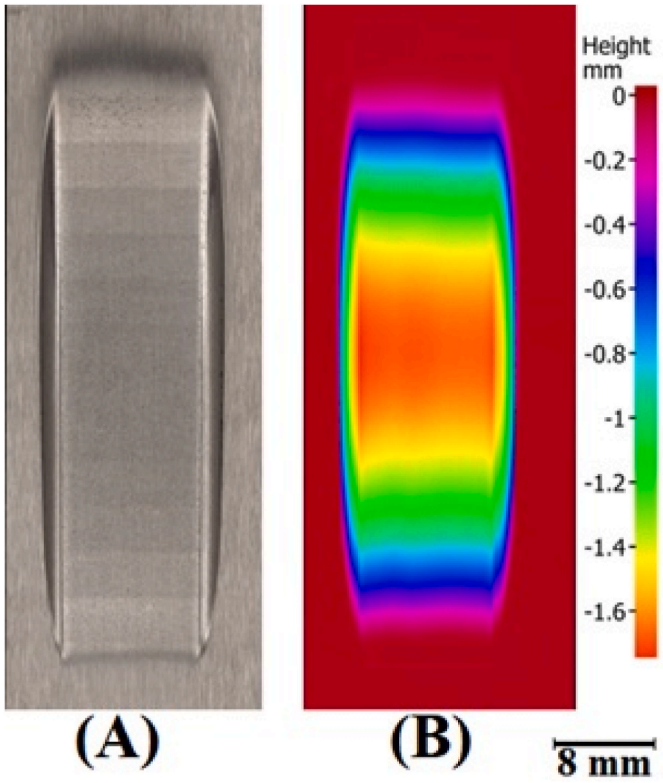

Fig. 9. EBM Ti64 extreme wear scar: (A) ETi64; (B) ETi64 heightmap.

standard, the ETi64 samples produced an extreme version, having very deep wear scars and wear marks caused by the contact of the rubber wheel with the sample (marked as "wheel contact wear" in Fig. 8). Fig. 9 shows the height map for a typical ETi64 sample.

Following these preliminary results, it was decided to reduce the test duration for EBM Ti64 samples to 2000 cycles (Test Method B) while continuing to use Test Method A (6000 cycles) for Ti64 samples.

3.5. Ti64 wear scars

The Ti64 had wear scars (Fig. 10), which showed rolling wear marks (detail B) in the centre that transitioned to a smaller number of long, parallel scratches towards the region where the sand exits the contact (detail C).

The cross-section of the central region of the wear scar is shown in Fig. 11. This image was obtained using a conventional microscope and cross-polarized lens. Part (A) of Fig. 11 shows an overview of the wear scar region, showing a wavy surface and deformed microstructural layer. Part (B) shows further details in the centre of the wear scar, where pits are visible as a result of removed material. Part (C) illustrates that the deformed layer extends to a depth of approximately 10 μm beneath the wear scar.

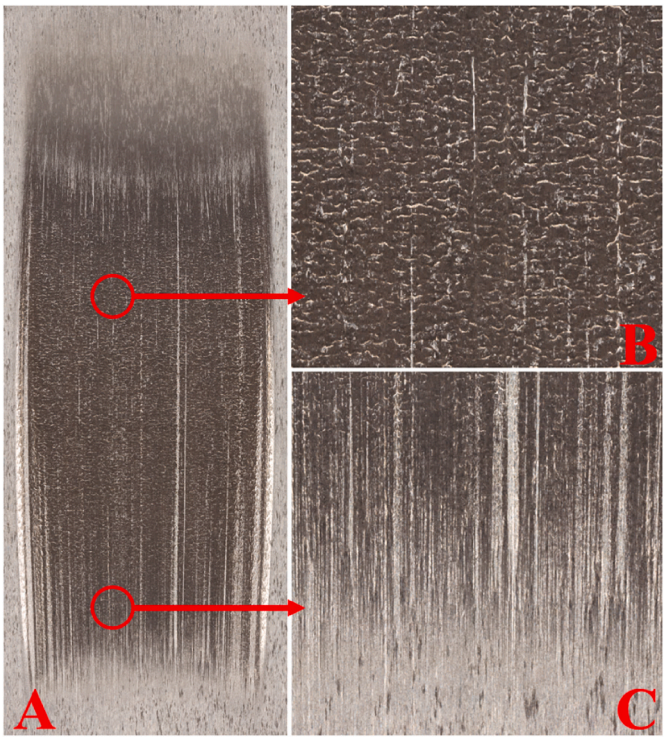

Fig. 10. (A) Ti64 typical wear scar; (B) Rolling marks; (C) Scratches.

3.6. EBM Ti64 wear scars

Following Test Method B (2000 cycles), the ETi64 samples were performed and the wear scars presented a more regular shape, with more clearly defined wear regions. A typical wear scar for the ETi64 samples is presented in Fig. 12.

The wear scars observed on ETi64 samples after 2000 cycles presented similar features to those seen on the Ti64 samples after 6000 cycles. The top section of the wear scar (detail B) shows rolling marks in the shape of waves and a concentration of scratches in the bottom part of the wear scar (detail C).

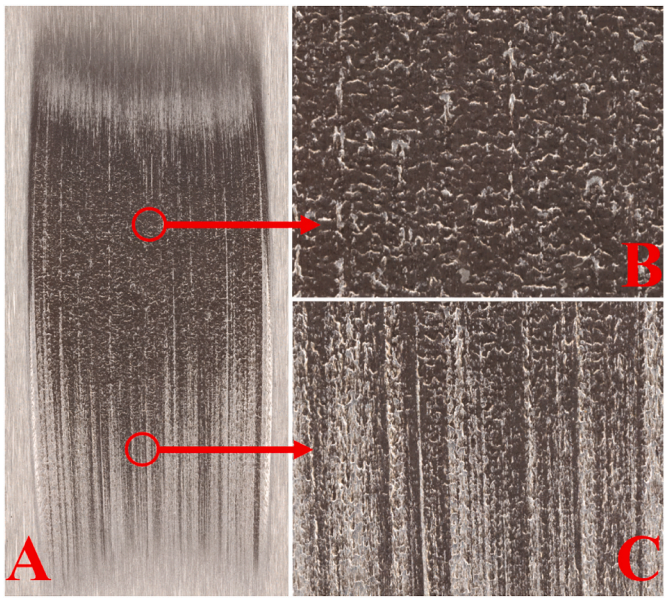

Fig. 12. (A) ETi64 typical wear scar for; (B) Rolling marks; (C) Scratches.

The analysis of the cross-section of a typical ETi64 wear scar is presented in Fig. 13, being composed of two micrographs acquired using cross-polarised lens in a conventional microscope. Two different objectives were used: (A) using 20x lens, and (B) & (C) using a 50x lens. In Part (A) the lamellar microstructure can be seen, with a narrow, deformed sub-surface layer. Part (B) shows further detail of the centre of the wear scar, with small pits evident as a result of removed material. Part (C) indicates that the thickness of the deformed layer, beneath the wear scar, was approximately 5 μm.

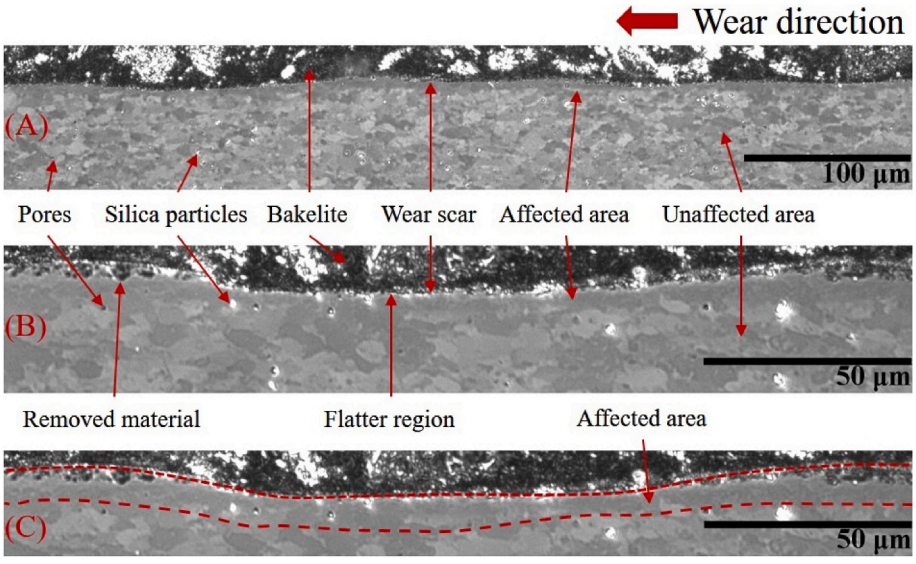

Fig. 11. Ti64 wear scar cross-section micrograph detail: (A) 20x micrograph; (B) 50x micrograph; (C) Affected area detail.

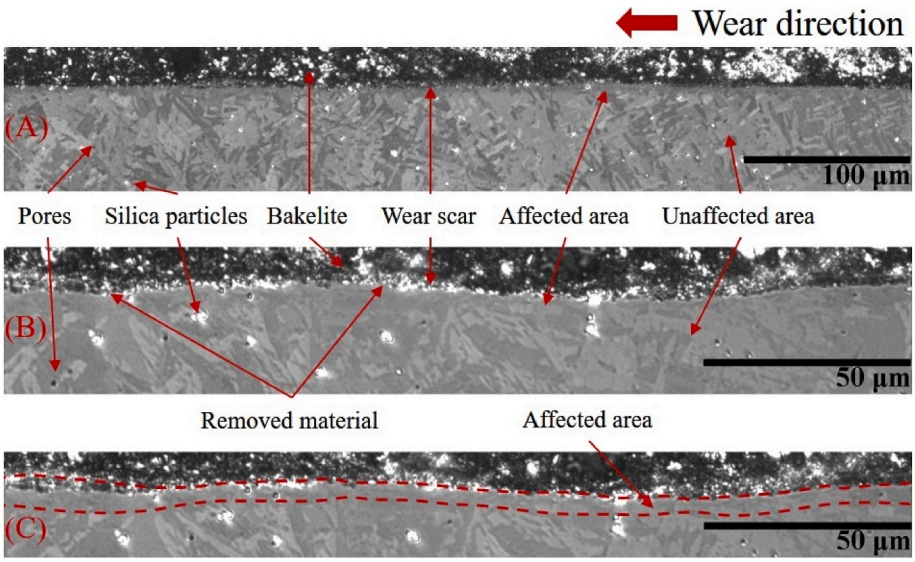

Fig. 13. ETi64 wear scar cross-section micrograph detail: (A) 20x micrograph; (B) 50x micrograph; (C) Affected area detail.

4. Discussion

In this work, the titanium samples were tested without any further heat treatment, being the material treated as an "off-the-shelf" solution, thus no custom parameters were used in the printing of the EBM samples. This was deemed to be suitable as an initial attempt since the development of own parameters in manual mode in the E-Beam equipment would need to be part of further study of the process. Prepared samples were submitted to Vickers macro- and micro-hardness testing, to verify the consistency of said material and determine whether there were significant microstructural scale effects contributing to their indentation resistance. As shown in Tables 2 and 3, all the groups of sample sets presented good repeatability, and no significant difference in the macro- and micro-hardness for both the conventionally and EBM obtained Ti64.

Microstructural characterisation revealed the differing microstructures resulting from the two tested manufacturing methods. As expected, the conventionally obtained Ti64 microstructure was composed globular α grains (Fig. 5) while the EBM samples showed lamellar α+β grains (Fig. 6) and increased porosity (6.8 times as many pores than the conventional sample, Table 5). It is important to note that the features like porosity and grain size can vary substantially, depending on the chosen EBM process parameters. Briefly, this is partly due the heat source being composed of electrons and finding an optimum melt efficiency being difficult to achieve. Variables such as the total scan length for the beam to travel, the number of components that are being melted simultaneously and preheating temperature, are some of the variables that may affect the melting spot quality and, therefore, the melt. As the current work does not involve parameter optimisation, the effect of these variables will be left for further study.

Abrasive wear tests were used to evaluate the wear resistance of the studied alloys. In the case of the EBM samples, the standard ASTM G65 Test Method A caused the samples to experience extreme wear, which produced a wear scar so deep that the sand flow was concentrated in the centre of it and led to the wheels contacting the side of the samples (Fig. 9), wearing the sample and the rubber patch of the wheel at the same time. The contact of the wheel with the samples surface damaged the corners of the wheel and rendered the results to be invalid, since the wear scar did not present an even shape. Due to this extreme wear behaviour and the damage caused to the rubber wheel, the EBM obtained samples were then submitted to a shorter duration abrasive wear test (defined as Test Method B in ASTM G65), having the duration of the test reduced to one-third that of Test Method A, for a total of 2000 revolutions. The conventionally obtained Ti64 samples were subjected to Test Method A, which presented repeatable wear results. As is subsequently described, the macroscopic wear features observed from both sets of tests were broadly similar, which indicated that the same dominant wear mechanism was taking place. While identical test conditions are preferable, the comparison of wear resistance between Ti64 (Test Method A) and EBM Ti64 (Test Method B) presented here is considered to be valid.

When comparing the wear scars for conventional Ti64 (Fig. 10) and EBM Ti64 (Fig. 12) some differences are seen. In Fig. 10 (detail B), the Ti64 presents fewer scratches, with wavy but roughly horizontal deformation marks dominating. These are a result of three-body interactions and appear due to the rolling motion of the abrasive on the surface of the wear scar region. As the abrasive particles move towards the exit of the contact (detail C) they tend to slide and, hence, form long, parallel scratches that are typical of a two-body abrasion mechanism.

For the ETi64 samples (Fig. 12), similar wear regions were seen, with some wavy, roughly horizontal deformation marks visible (detail B), giving way to long parallel scratches (detail C). However, the relative sizes of these regions were seen to differ significantly from the conventional Ti64 samples, with more of the wear scar dominated by scratches. These scratches were surmised to result from the larger quantity of pores in the EBM material, which increased the chance of abrasive particles catching and then ploughing/cutting the material and/or acting as stress concentrators from which larger defects may grow to accelerate the rate of material loss. This action not only leads to more scratches but deeper scratches, corresponding to the significantly higher wear rates (+120% comparing ETi64 with Ti64 and accounting for the shorter test duration) determined from the volumetric data (Table 7).

From the cross-section micrographs for Ti64 (Fig. 11) and EBM Ti64 (Fig. 13) further details of the differing wear damage was seen. The response of the predominantly globular α structure (in the conventional material) most notably differs from the lamellar α+β structure (in the EBM material), in terms of the depth of the plastically deformed layer generated from the wear process. In the Ti64 material this was observed to extend roughly 10 µm from the worn surface, while in the ETi64 material the deformed layer was around 5 µm thick. While a shallower deformed layer might be taken to indicate greater strengthening in samples with similar microstructures (e.g. smaller but still globular grains), no significant difference was observed in indentation hardness between the conventional and EBM samples.

It is worth noting that EBM parts and, AM materials in general,

typically lack isotropy. As in the case of the samples tested here, they come from an orientation where the prior β-grain (from solidification) form a columnar morphology, left from the solidification gradient. Such anisotropy, to some extent, cause a variation of properties widely reported in literature [13]. Since the wear testing was carried out on the same plane as the elongated morphology (referring to the build orientation indicated in Fig. 1), the contact surface would lie, approximately, on the same plane. This effect has been attributed, to some extent, to a potential low level of mechanical properties [14].

The primary type of wear expected by the ASTM G65 abrasive wear test is low-stress three-body abrasion, which agrees with the results found on most of the wear scars generated in this work. The deeper scratch marks represent a considerably smaller part of the wear scar and can be attributed to the poor wear resistance of the titanium alloy itself, which facilitates the occurrence of scratches due to ploughing happening. This phenomenon can be seen more frequently on the EBM obtained samples as shown.

Even though the test duration used for the EBM samples was one-third that applied to the conventional samples, the comparison of it being an option of "of-the-shelf" (i.e. not tailoring the EBM parameters to a specific application) solution is still valid and worth taking into consideration. The customization of the parameters for EBM printing is both time and budget consuming, which should be considered when choosing materials and process solutions for any specific application. In this study, when directly comparing these two variants of Ti–6Al–4V alloy as "ready solutions", the conventional Ti64 arguably presents an advantage over the EBM material as, for the same hardness, it offers significantly greater abrasive wear resistance.

A limitation of the work presented here is that it is hard to compare the volume loss across the specimens directly, rather than by means of a wear rate and assumption that the wear would accumulate linearly between the test lengths used. Further testing with directly comparable test conditions, albeit not conforming to ASTM G65, would add confidence. It is believed, however, that it is useful to report these initial findings of the relative wear performance for nominally the same hardness as presented here.

5. Conclusions

The conclusions of this study, comparing the abrasive wear resistance of Ti–6Al–4V alloy produced conventionally and by electron beam melting (EBM) are.

1. There was no significant difference in the Vickers macro-hardness and micro-hardness of the alloy produced by EBM compared to casting.
2. The EBM samples presented an average of 6.8 times as many pores per unit area than the cast Ti64 samples.
3. The EBM obtained samples have significantly worse abrasive wear resistance than the more conventional cast Ti64 alloy, with comparable volumetric wear rates determined to be 120% greater.
4. The wear scars for all samples showed a combination of three body abrasion (rolling marks) and ploughing, that resulted in long, parallel scratches along the wear scar length.
5. The dominant wear damage observed in cast samples resulted from three-body abrasion (rolling marks), while for EBM samples it resulted from two-body abrasion (deep, parallel scratches).

Declaration of competing interest

The authors declare that they have no known competing financial interests or personal relationships that could have appeared to influence the work reported in this paper.

Acknowledgements

The authors gratefully acknowledge the kind support of: Brazilian National Council for Scientific and Technological Development (CNPq) (Science Without Borders 201534/2015-0) (financial support of PH), The University of Leicester Advanced Microscopy Centre (SEM facilities), and EPSRC Future Manufacturing Hub in Manufacture using Advanced Powder Processes (MAPP) (EP/P006566/1) (financial support of EH-N and EBM processing facilities).

Appendix

Figure A1 and A2 show example images obtained during the analysis of the pores in the microstructure of the Ti64 and ETi64 respectively. A Clemex image acquisition system was used, the software of which to measure the pores found in the scanned area.

Fig. A1. Example image used to analyse the pores (the dark spots) found in the microstructure of Ti64.

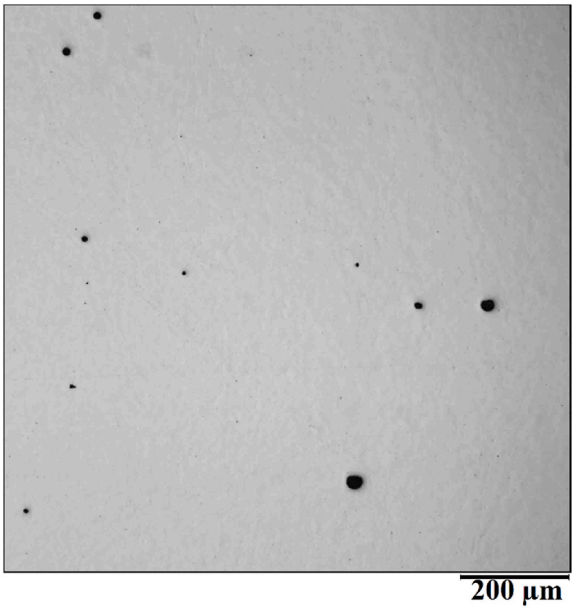

Fig. A2. Example image used to analyse the pores (the dark spots) found in the microstructure of ETi64.

References

[1] K.G. Budinski, Tribological properties of titanium alloys, Wear 151 (1991) 203–217, https://doi.org/10.1016/0043-1648(91)90249-T.
[2] K. Gu, J. Wang, Y. Zhou, Effect of cryogenic treatment on wear resistance of Ti-6Al-4V alloy for biomedical applications, J. Mech. Behav. Biomed. Mater. 30 (2014) 131–139, https://doi.org/10.1016/j.jmbbm.2013.11.003.
[3] J. Matthew J. Donachie, Titanium - A Technical Guide, second ed., ASM International, 2000.
[4] L. Kunčická, R. Kocich, T.C. Lowe, Advances in metals and alloys for joint replacement, Prog. Mater. Sci. 88 (2017) 232–280, https://doi.org/10.1016/j.pmatsci.2017.04.002.
[5] M. Sandomierski, T. Buchwald, A. Patalas, A. Voelkel, Improving the abrasion resistance of Ti6Al4V alloy by modifying its surface with a diazonium salt and attaching of polyurethane, Sci. Rep. 10 (2020), 19289, https://doi.org/10.1038/s41598-020-76360-3.
[6] C. Jiang, J. Zhang, Y. Chen, Z. Hou, Q. Zhao, Y. Li, L. Zhu, F. Zhang, Y. Zhao, On enhancing wear resistance of titanium alloys by laser cladding WC-Co compsite coatings, Int. J. Refract. Metals Hard Mater. 107 (2022), 105902, https://doi.org/10.1016/j.ijrmhm.2022.105902.
[7] C. Chirico, A. Vaz Romero, E. Gordo, S.A. Tsipas, Improvement of wear resistance of low-cost power metallurgy β-titanium alloys for biomedical applications, Surf. Coating. Technol. 434 (2022), 128207, https://doi.org/10.1016/j.surfcoat.2022.128207.
[8] S.S. Al-Bermani, M.L. Blackmore, W. Zhang, I. Todd, The origin of microstructural diversity, texture and mechanical properties of electron beam melted Ti-6Al-4V, Metall. Mater. Trans. 41 (2010) 3422–3434, https://doi.org/10.1007/s11661-010-0397-x.
[9] Standard Test Method for Measuring Abrasion Using the Dry Sand/Rubber Wheel Apparatus - G65-16, 2016, https://doi.org/10.1520/G0065-16.
[10] S.L. Semiatin, T.R. Bieler, The effect of alpha platelet thickness on plastic flow during hot working of Ti-6Al-4V with a transformed microstructure, Acta Mater. 49 (2001) 3565–3573, https://doi.org/10.1016/S1359-6454(01)00236-1.
[11] E. Hernández-Nava, C.J. Smith, F. Derguti, S. Tammas-Williams, F. Léonard, P. J. Withers, I. Todd, R. Goodall, The effect of density and feature size on mechanical properties of isostructural metallic foams produced by additive manufacturing, Acta Mater. 85 (2015), https://doi.org/10.1016/j.actamat.2014.10.058.
[12] G. Lutjering, J.C. Williams, Titanium, second ed., Springer, Heidelberg, 2007.
[13] A.A. Antonysamy, J. Meyer, P.B. Prangnell, Effect of build geometry on the ??-grain structure and texture in additive manufacture of Ti6Al4V by selective electron beam melting, Mater. Char. 84 (2013) 153–168, https://doi.org/10.1016/j.matchar.2013.07.012.
[14] A.H. Chern, P. Nandwana, R. McDaniels, R.R. Dehoff, P.K. Liaw, R. Tryon, C. E. Duty, Build orientation, surface roughness, and scan path influence on the microstructure, mechanical properties, and flexural fatigue behavior of Ti–6Al–4V fabricated by electron beam melting, Mater. Sci. Eng. 772 (2020), 138740, https://doi.org/10.1016/j.msea.2019.138740.